Sensory-Motor Manifold Structure Induced by Task Outcome: Experiments with Robonaut

Richard Alan Peters II
and Robert E. Bodenheimer
Center for Intelligent Systems
Vanderbilt University School of Engineering
Nashville, TN 37235
Email: Alan.Peters@Vanderbilt.Edu

Odest Chadwicke Jenkins
Department of Computer Science
Brown University
Providence, RI 02912-1910
Email: cjenkins@cs.brown.edu

***Abstract*— Experiments were performed with Robonaut to determine if repeated teleoperation through a task could delineate a manifold in the robot's sensory-motor state-space (SMSS) that was separable by the outcome of the task. A teleoperator guided the robot through 13 trials of a pick and place task. By design, in 5 of the trials were successful and 8 were not. A time series of instantaneous sensory-motor state vectors was recorded at 8Hz from the robot throughout the trials. Support Vector Machine (SVM) analysis suggested that the individual vectors were separable with a 70% probability if both sensory and motor information were used. The analysis revealed, however, little structural information beyond the promise of reasonable separability. Therefore, dimensionality reduction techniques were applied. These embed high-dimensional vectors into a lower dimensional space where patterns may be discernible. Singular Value Decomposition, Multidimensional Scaling, and Spatio-Temporal Isomap (STI) analysis of the time series revealed a 3D structure within the SMSS that was dependent on, and separable by task outcome. An STI embedding generated by 2 successful and 4 unsuccessful trials was seen to be sufficient for the projection and classification of the remaining trials. A comparison of that result with the SVM classification demonstrated that STI outperformed SVM. It is conjectured that STI's reliance on the temporal evolution of the time-series gave it the advantage over the SVM analysis which was time independent. It was also found that Robonaut's haptic sensory data degraded the outcome separability if used without processing. However, lateral inhibition of the haptic signals significantly enhanced separability in both the SVM and STI analyses.**

I. Introduction

When a robot is programmed through demonstration or controlled through teleoperation, its resultant sensory-motor data stream can form discernable patterns in the vector space that contains them, the sensory-motor state space (SMSS). The patterns reflect both measurable effects on the environment of the robot's actions and its motor reactions to sensory input. Thus, the patterns emerge from a closed-loop interaction between robot and environment. This phenomenon was demonstrated with a simple mobile manipulation robot by Pfeifer in 1999 [1].

The SMSS has dimension equal to the number of scalar signals that can be recorded while the robot operates. But, the effective dimension of the pattern may be much smaller, depending on the number of independent variables that dominate during the interaction. In cases of repetitive, constrained motion by the robot (for example repeatedly reaching toward and grasping an object) the dominant variables tend to trace closed manifolds in the SMSS. Closure makes sense because during exact repetitions of a task the trajectory through SMSS would repeat itself. If the task is repeated with some variations, say under different initial conditions in robot or environment, the trajectory does not repeat itself exactly. Instead, a family of trajectories lies on a closed surface in the SMSS, displaced from one another along directions that correspond to the variations. By having the robot perform the same task under different initial conditions, limits on the manifold might be discerned.

This paper reports on an experiment designed to elicit a bifurcated manifold and to determine if it could be used to to classify further repetitions of the task. The experiment, performed with Robonaut, was to reach for, grasp, pick up, move, and release an object, then return to the starting position. The teleoperator caused the robot to succeed during some tasks and fail during others. To determine if the SMSS vectors in the recorded data could be classified with a probability greater than chance, a Support Vector Machine (SVM) Analysis was used. Since the task had two possible outcomes over quasi-periodic repetitions the dominant patterns in the SMSS should be low dimensional – at least 2D, perhaps 3D. To elucidate any such manifolds, dimensionality reduction algorithms were applied to the SM time-series. In particular, Principal Components Analysis (PCA), Multidimensional Scaling (MDS), and Spatio-Temporal Isomap (STI) were used to learn the manifold structure.

II. Previous Work

In [2] a single SMSS trajectory was learned over six trials that could later be performed autonomously with success in the face of small variations in the environment or perturbations of the goal. Later it was shown that sets of such learned trajectories could be interpolated to provide intermediate results [3]. The formation of low dimensional manifolds in the Robonaut SMSS as a consequence of task repetition was reported in [4]. In addition to Pfeifer [1], many others have studied the extraction of SMC parameters, including Cohen [5], Grupen [6], Lungarella [7], and Peters [8]. Te Boekhorst et al. [9]

Fig. 1. Robonaut, NASA's space capable humanoid robot.

have shown that SMC reduces the intrinsic dimensionality of the problem of category learning by a robot.

The use of motion data to plan robotic motion is a problem that has been studied by Matarić [10], Jenkins and Matarić [11], Ude et al. [12], Pollard et al. [13], and Atkeson et al. [14]. Matarić and Jenkins have enabled a simulated humanoid to learn unconstrained motion patterns from human motion-capture data.

Jenkins developed Spatio-temporal Isomap for the creation of new motions through the interpolation of learned trajectories [15]. STI is an extension of Isomap [16], one of a number of dimensionality reduction techniques including Principal Component Analysis [17], and the related Singular Value Decomposition, both of which are textbook approaches, Multi-dimensional Scaling [18] and Locally Linear Embedding [19]. Application of dimensionality reduction to robotics has been done by Asada [20] MacDorman [21], and others.

Support vector machines are described in several textbooks including [22]. Pelossof, et al., [23] studied the learning of stable grasps by SVMs.

III. Robonaut

Robonaut is NASA's space-capable, humanoid robot. (Fig. 1). Robonaut was developed by the Dexterous Robotics Laboratory of the Automation, Robotics, and Simulation Division of the NASA Engineering Directorate at Lyndon B. Johnson Space Center in Houston, Texas [24]. Each seven degree of freedom (DoF) Robonaut arm is approximately the size of a human arm. Each of those mates with a 12-DoF hand to produce a 19-DoF upper extremity.

Robonaut's sensors include a color, stereo camera platform embedded in a head that is mounted on a 3-DoF neck, and

TABLE I

Signals Recorded from Robonaut.

Signal	Dimension
End-effector 4×4 position	16
Arm orbit angle	1
Arm joint positions	7
Finger joint positions	12
6-axis force on wrist	6
6-axis force on shoulder	6
Arm joint torques	7
Force on fingers	5
Finger joint torques	12
Hand tactile sensors	33

binaural microphones located on opposite sides of the head, parallel to the stereo camera baseline. The two hand/wrist modules contain 98 sensors for feedback and control. Each DoF has a motor position sensor, a joint force sensor, and a joint absolute position sensor. The two arm modules contain 90 sensors. Each actuator contains a motor incremental position sensor, redundant joint torque sensors, redundant joint absolute position sensors, and four temperature sensors distributed throughout the joint. Each arm employs relative optical encoders in five of its joints. The encoders reside on the motor side of the gear train and have resolutions ranging between 200 and 1000 counts per degree of arm motion. (See [25] for a more detailed description of the Robonaut mechatronics.) The data signals that were recorded from Robonaut during teleoperation are listed in Table I. The ones that were actually used for this experiment are in italic type. The resulting 105-dimensional vector time-series was recorded at a nominal rate of 8Hz.

Although Robonaut is physically capable of autonomous operation it is most often controlled directly via teleoperation. (See [24] for a detailed description.) Significantly, haptic sensations and joint forces cannot be reflected from the robot back to the teleoperator, who guides the robot based on vision alone. Given its sensor suite, the robot is capable of "feeling" for itself the effects of its actions. To enable the robot to act and react on its own sensory motor coordination is one of the motivations behind the research reported herein.

IV. Manifolds in SMSS and Outcome Classification

In [4] it was reported that in Robonaut's SMSS closed manifolds can be formed by task repetition. If the robot always starts the task in a similar SM state, the initial part of the manifold should be small, highly localized. If the task diverges into multiple variations or outcomes, one would expect the manifold to ramify accordingly over the course of the repetitions. In particular, if the task has the binary outcome set $\{\text{success}, \text{failure}\}$, and if the trials are performed to include examples of each, one would expect the manifold to bifurcate. If this were shown to be true, later repetitions of the task should map to the manifold in such a way that success or failure could be detected. That is, by learning the manifold

under teleoperation, the robot could then assess the outcome of later autonomous execution by observing the branch of the manifold upon which its SM state projects.

A. Support Vector Machines

The SVM algorithm operates by mapping a given training set into a high-dimensional *feature space* and finding a hyperplane that separates the data into classes. To construct an optimal hyperplane, the SVM minimizes a particular error function, and in this work, we use the C-SVM classification [26]. Given a training set of attribute-label pairs (x_i, y_i), where $i = 1 \dots l$, training vectors $x_i \in \mathbb{R}^n$ and $y_i \in \{+1, -1\}^l$, C-SVM minimizes the following error function:

$$\min_{\mathbf{w},b,\xi} \frac{1}{2}\mathbf{w}^T\mathbf{w} + C\sum_{i=1}^{l}\xi_i$$

subject to $y_i(\mathbf{w}^T\phi(x_i) + b) \geq 1 - \xi_i$. The training vectors x_i are mapped to a higher dimension by the kernel function ϕ. Given a sufficiently high dimension and an appropriate, nonlinear kernel ϕ, any data set can be mapped by ϕ into the high dimensional space such that a hyperplane separating the data into its appropriate categories exists. C is the penalty parameter of the error function, which controls the trade-off between allowing training errors and forcing rigid margins, $\mathbf{w}$ is a vector of coefficients, b is a constant, and ξ_i are parameters for handling non-separable input data. We chose to use a radial basis function (RBF) kernel having the form $\phi = e^{-\gamma\|x_i - x_j\|^2}$, where $\gamma > 0$.

B. Manifold Learning through Dimensionality Reduction

We assume sensorimotor observables – the time series – are intrinsically parameterized by a lower dimensional embedding. The embedding provides a mapping $=\phi(\mathbf{y})$ between intrinsic parameters and observations, realizing intrinsic coordinates $\mathbf{y}_k : \{1, 2, 3, \dots N\} \rightarrow \mathbb{R}^n$ for the input data where $n < N$. Such a latent parameterization could be uncovered by applying dimensionality reduction techniques such as Principal Components Analysis [17]. PCA involves an eigendecomposition on a linear covariance matrix to find an orthogonal subspace of principal components that compactly approximate the input data. Singular value decomposition, which we have used, provides an equivalent projection.

Multidimensional scaling [18] is another approach where pairwise distances, rather than linear covariance, are preserved. Given the distance between all input data pairs $D_{\mathbf{S}_j,\mathbf{S}_k}$, MDS produces embedding coordinates that minimizes the error $E = |D_s - D_y|_{L^2}$, where D_s and D_y are respectively the pairwise input and embedding space distance matrices. Essentially, MDS produces embedding coordinates that preserves the distance metric as much as possible. Isomap [16] uses a geodesic (Dijkstra shortest-path) distance metric with MDS. The resulting embeddings avoid "short-circuiting" problems associated with Euclidean distance between non-proximal data pairs.

These techniques are not ideally suited for time-series analysis data because they assume the input are i.i.d. – independent samples from the same manifold parameterization. Time-series data are not independent, but rather sequentially ordered samples from an underlying spatio-temporal process. To add a time-dependency to MDS, we use a "windowed MDS" procedure, where each input data object is a temporally extended window of observations. Adding time as another dimension This serves to disambiguate spatially proximal data pairs that are different phases of a temporal process. But it does not detect the temporal coincidence of spatially distant data pairs that are in phase with respect to the temporal process. Spatio-temporal Isomap [27] accounts for both proximal disambiguation and correspondence over a distance.

V. The Experiment

Robonaut was teleoperated through a task that involved reaching, grasping, and moving an object. Thirteen trials of the task were performed. In 5 of the trials the task was completed successfully; in 8, it was not (Figs. 2,3). The object was an upright chisel on a stand. A simple distal closure grasp could be used. A trial was a success if the robot formed a stable grasp on the object, lifted it, moved it to another position where it released it. A trial was a failure if the robot knocked the object over without forming a grasp or if the robot let slip the object upon lifting it.

The 3-space motion trajectories of the end-effecter are shown in Fig. VI (a). The successful trials are in blue and the unsuccessful in red. The starting point of all trials was near $(x, y) = (38, 42)$. The chisel was randomly placed near $(x, y) = (58, 42)$. There was more variation in the object placement than the starting position. In every successful trial the robot moved the object to a position near $(x, y) = (38, 72)$ where it released it and returned to the starting area in a predominately y-axis direction. In all the unsuccessful trials the robot moved its end-effecter beyond the object position and returned in a predominately y-axis direction.

It is clear from the figure that if end-effecter position or arm joint angles were used to train the manifold, they would dominate its structure and make classification by any method trivial. Less obvious from the diagram, but quite evident in the motor signals, the wrist position differed significantly between the two classes on a segment of the trajectories. We excluded that information from the analysis and used only end-effecter related signals. Thus classification of the outcome was dependent solely on sensory information from the wrist to the finger tips and on motor information from the fingers alone (Table I). All 110 sensory and motor channels were sampled at 8Hz. The exclusion of arm-related signals left a 68-dimensional vector time series. The number of vectors in a trial varied from 100 to 215 with a median length of 161 vectors.

A. Signal Processing

In the following, $\mathbf{s}(k) \in \mathbb{R}^n$ is the sensory-motor vector provided by the robot at a time index, k. Vector $\mathbf{s}(k)$ contains n

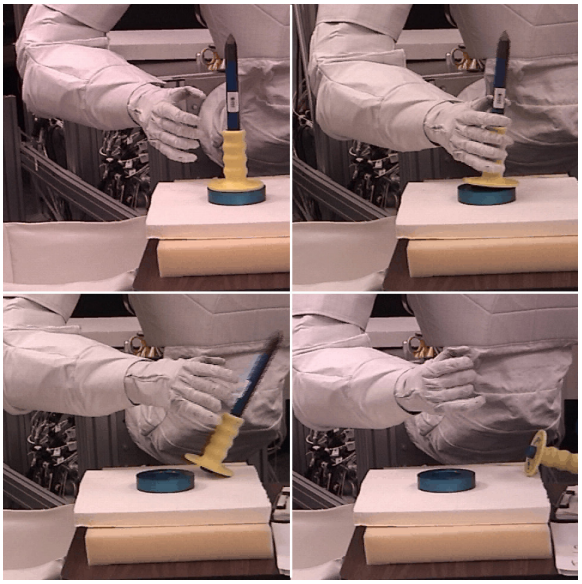

Fig. 2. Unsuccessful grasp sequence.

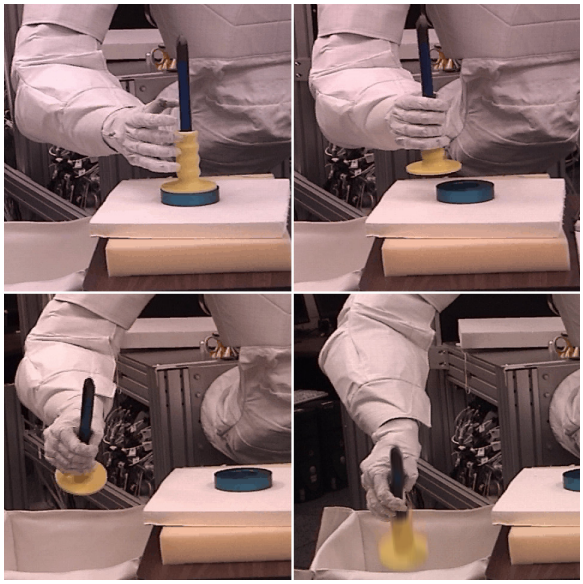

Fig. 3. Successful grasp sequence.

scalars, $[s_1(k), \ldots, s_n(k)]$ each of which is the instantaneous value of a sensor output or motor control variable. Let $\mathbf{s} = \{\mathbf{s}(k)\}_{k=1}^{m}$ denote an arbitrary vector time-series.

Each of the 68 data streams was normalized by its machine limits.

$$s_i(k) \leftarrow \frac{s_i(k) - \mu_i}{M_i - \mu_i}, \tag{1}$$

for all j, where μ_i is the actual minimum value that the sensor or control variable can take on (determined by the robot specifications) and M_i is the maximum.

One of the dimensionality reduction algorithms, SVD-PCA, further required that signal be mean shifted over the all iterations.

$$s_i(k) \leftarrow s_i(k) - E[s_i], \tag{2}$$

where $E[s_i]$ is the sample mean of the ith sensor over its entire duration (all trials). (The SVM analysis, MDS, and STI all used (1) as input.)

The analyses described below indicated that noise in the sensors was degrading the performance. In fact, the finger force and torques appeared completely random as did the 33 individual haptic sensor streams. We found, however, that the haptic data was a strong indicator of grasp success if the ∞-norm of 33-dimensional vector was used. That is simply the maximum of the values in the haptic vector at any one time,

$$\|\mathbf{s}(k)\|_{\infty} = \max\{s_i(k) \mid i = 1, \ldots, n\}. \tag{3}$$

That corresponds to a winner-take-all strategy or a nonlinear lateral inhibition of the sensors. Nonlinear smoothing in the time domain with a morphological open-close [28] filter further improved the result. All the analyses were performed on both the 68-dimensional, normalized but otherwise unprocessed, sensory-motor data and a 19-dimensional subset that included the finger position vector, the force and torque on the wrist and the scalar haptic signal just described.

B. SVM Analysis

Support vector machine analysis was used to estimate the probability that any single vector from any single trial could be identified correctly as coming from a successful trial. An SVM classifier was built from a subset of the trials then used to classify the vectors in the remaining trials. The analysis was performed using motor data alone, sensory data alone, and sensory and motor data together.

A radial basis function (RBF) kernel was used for all the tests. The associated parameters, margin $C = 32$ and RBF exponent $\gamma = 8$ were determined through a grid search over $C = 2^{-5}, 2^{3}, \ldots, 2^{15}$ and $\gamma = 2^{-15}, 2^{-13}, \ldots, 2^{5}$ using $4\times$ cross-validation as suggested in [29].

To estimate the classification accuracy with a maximum possible confidence, a SVM classifier f was generated for every possible combination of 5 successful trials and 8 unsuccessful trials such that each classifier was built from at least one trial of each type. There are 7904 such combinations and, therefore, classifiers. Then each classifier was tested with the vectors from the trials that were not used to build it and the number of correctly labelled vectors was recorded. Based on the statistics of the exhaustive test, a single classifier was built from 2 successful and 4 unsuccessful trials. The vectors that were labelled incorrectly by the classifier were recorded and later compared to the results of the dimensionality reduction algorithms.

C. Manifold Learning

The time-series of the 13 trials were analyzed using Singular Value Decomposition, Multidimensional Scaling, and Spatio-Temporal Isomap. The three most significant dimensions of contours were plotted such that the first two principal directions defined the xy-plane. If the SMSS manifold were to

TABLE II
PERCENT VECTORS CORRECTLY CLASSIFIED BY SVM

Sensory Data	Motor	Sensory	Sensory-Motor
Unprocessed	69	64	63
Processed	69	67	70

exhibit a significant bifurcation, it should be evident in that plane.

VI. RESULTS

Table II displays the aggregate results of the exhaustive SVM tests for classifiers built from 2 successful and 4 unsuccessful trials applied to the unprocessed and the processed data, further broken down into motor signals alone, sensory signals alone, and sensory motor together. When using the data directly from the robot (normalized but otherwise unprocessed), the motor data alone yields a better classifier than either the sensory data or the sensory-motor together. Applying the nonlinear noise filter to the haptic signals resulted in the sensory-motor classifier being the best. But was only slightly better. Moreover a correct classification of only 70% is not particularly good. These probabilities are the averages over the 700 models built from 2 successful and 4 unsuccessful trials. The best model of that type correctly classified the processed sensory-motor data with 87% accuracy and the worst with 44%.

To determine which vectors were being misclassified, we selected a single classifier, the one trained on trials 1, 2, 4, 5, 10 and 13. Trials 2 and 4 were successful. The other four were not. That classifier had 73% accuracy when applied to the vectors in the 7 trials not used for model, *viz.* 3, 6, 7, 8, 9, 11, and 12, with trials 3 and 11 the successful ones. Fig. VI (a) shows the misclassified vectors plotted as '$*$'s on the end-effecter trajectory. Many of those points were along trajectory 3 for reasons unknown.

We applied the 3 dimensionality reduction procedures to all 13 trials in one continuous time series. The top row of Fig. VI shows results for the full 68-D unprocessed time series. The bottom row shows them for the 19-D processed time series. The first panel in each row, (a) and (d), depict the windowed distance matrix from which the MDS and STI embeddings were computed. Panels (b) and (e) show the SVD, (c) and (f) the MDS, and (d) and (h) the STI embeddings of the time series. All 6 of these clearly bifurcate along task outcome in the principal plane. The manifold traced by the STI embedding of the processed data forms has the best separation and the most symmetric structure.

Fig. fig:SMSMTrajs shows the STI embedding of the various combinations of sensor and motor data. The sensory motor manifold in (d) is apparently smoother and more easily separable than either (b) or (c). Manifold (d) is very similar in structure to the pure motor manifold (a). The sensory-motor manifold appears to be more compact on its unsuccessful branch than does the motor manifold. But the difference is slight.

Fig. VI (b) and (c) compare the SVM classification to classification by STI. Panel (b) is a plot of the SVM misclassified vectors on the STI embedding. Most of the misclassifications occur in the reach phases of the tasks as would be expected, given causality. But the misclassification of trial 3's post grasp trajectory is also visible.

The thin contours in Fig. VI (c) comprise the STI embedding of trials 1, 2, 4, 5, 10 and 13 – those used to train the SVM. The thick lines show the projection of trials 3, 6, 7, 8, 9, 11, and 12, onto the manifold traced by the former. This shows that the manifold embedding created by STI using 6 trials of the task not only traces an outcome-dependent manifold, but also classifies the new data much more accurately than does the SVM classifier.

REFERENCES

[1] R. Pfeifer and C. Scheier, *Understanding Intelligence*. The MIT Press, Cambridge, MA, 1999.

[2] R. A. Peters II, C. L. Campbell, W. J. Bluethmann, and E. Huber, "Robonaut task learning through teleoperation," in *Proceedings of the 2003 IEEE International Conference on Robots and Automation (ICRA 2003)*, Taipei, Taiwan, Oct. 2003.

[3] C. L. Campbell, R. A. Peters II, R. E. Bodenheimer, W. J. Bluethmann, E. Huber, and R. O. Ambrose, "Superpositioning of behaviors learned through teleoperation," *IEEE Transactions on Robotics*, vol. 22, no. 1, pp. 1–13, Feb. 2006.

[4] R. A. Peters II and O. C. Jenkins, "Robonaut: manifold structures in sensory motor state space," in *Proceedings of the IEEE/RAS International conference on Humanoid Robots (Humanoids 2005)*, Tsukuba, Japan, Dec. 2005.

[5] P. R. Cohen and N. Adams, "An algorithm for segmenting categorical time series into meaningful episodes," in *Proceedings of the Fourth Symposium on Intelligent Data Analysis*, vol. 2189, 2001, pp. 198–207.

[6] J. A. Coelho Jr., J. H. Piater, and R. A. Grupen, "Developing haptic and visual perceptual categories for reaching and grasping with a humanoid robot," in *Proceedings of the First IEEE/RAS International conference on Humanoid Robots (Humanoids 2000)*, Sept. 2000.

[7] M. Lungarella, T. Pegors, D. Bulwinkle, and O. Sporns, "Methods for quantifying the information structure of sensory and motor data," *Neuroinformatics*, vol. 3, no. 3, pp. 243–262, Fall 2005.

[8] M. E. Cambron and R. A. Peters II, "Determination of sensory motor coordination parameters for a robot via teleoperation," in *Proceedings of the 2001 IEEE International Conference on Systems, Man, and Cybernetics*, vol. 5, Oct. 2001, pp. 3252–3257.

[9] R. Te Boekhorst, M. Lungarella, and R. Pfeifer, "Dimensionality reduction through sensory-motor coordination," in *Proc. of Joint Int. Conf. on Aritifical Neural Netwoks and Neural Information Processing*, 2003, pp. 496–503.

[10] M. J. Matarić, "Getting humanoids to move and imitate," *IEEE Intelligent Systems*, vol. 15, no. 4, pp. 18–24, July 2000.

[11] O. C. Jenkins and M. J. Matarić, "Performance-derived behavior vocabularies: data-driven acqusition of skills from motion," *International Journal of Humanoid Robotics*, vol. 1, no. 2, pp. 237–288, June 2004. [Online]. Available: http://www.cs.brown.edu/~cjenkins/papers/cjenkins_ijhr2004.pdf

[12] A. Ude, C. G. Atkeson, and M. J. Riley, "Planning of joint trajectories for humanoid robots using b-spline wavelets," in *Proceedings of the 2001 IEEE International Conference on Robotics and Automation (ICRA 2001)*, Apr. 2000, pp. 2223–2228.

[13] N. S. Pollard, J. K. Hodgins, M. J. Riley, and C. G. Atkeson, "Adapting human motion for the control of a humanoid robot," in *Proceedings of the 2002 IEEE International Conference on Robotics and Automation (ICRA 2002)*, May 2002, pp. 1390 – 1397.

[14] C. G. Atkeson, J. G. Hale, F. Pollick, M. J. Riley, S. Kotosaka, S. Schaal, T. Shibata, G. Tevatia, A. Ude, S. Vijayakumar, and M. Kawato, "Using humanoid robots to study human behavior," *IEEE Intelligent Systems*, vol. 15, no. 4, pp. 46–56, July 2000.

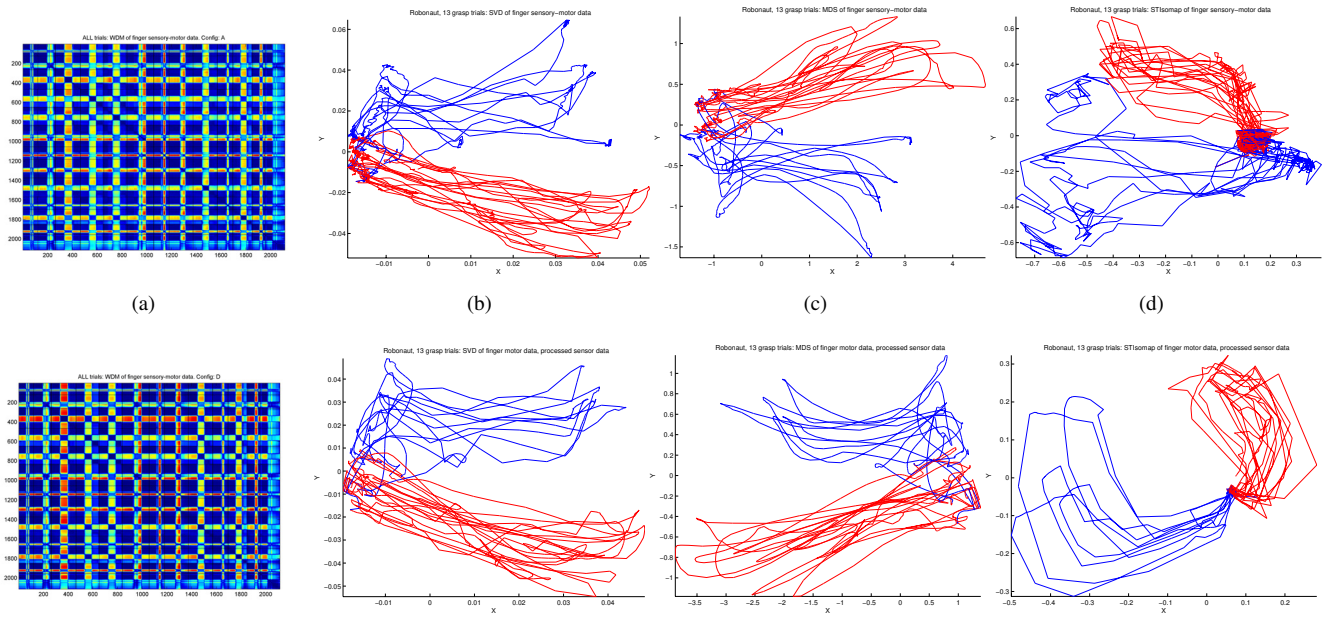

Fig. 4. In all the trajectory plots, blue corresponds to a successful, and red to an unsuccessful, trial. (a) - (d) were generated from the 68-dimensional normalized time series. (e) - (h) were generated from the 19-dimensional time-series with processing of the haptic signals. (a) Windowed distance matrix of the sensory-motor time series. (b) Trajectory embedded by SVD-PCA, (c) by MDS, and (d) by STIsomap. (e) Windowed distance matrix, (f) SVD-PCA, (g) MDS, (h) STI.

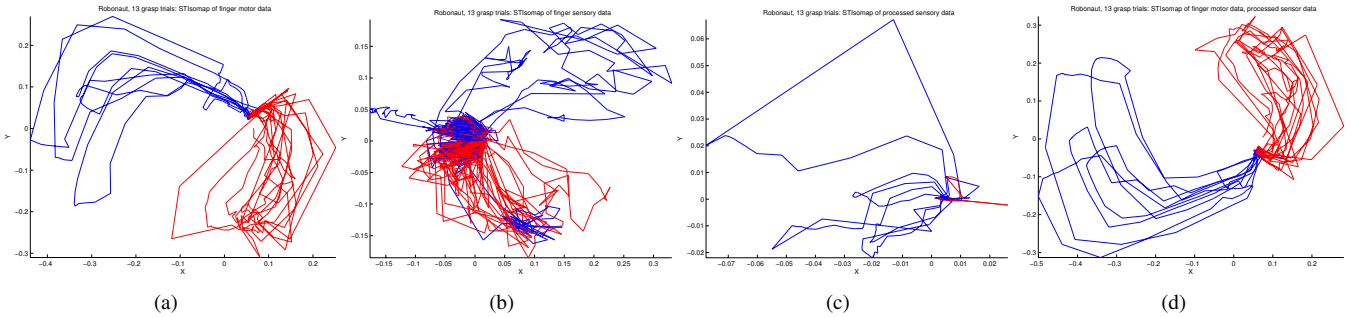

Fig. 5. (a)-(c) are examples of STI trajectories constructed from motor signals alone and sensory signals alone. In all the trajectory plots, blue corresponds to a successful, and red to an unsuccessful, trial. (a) unprocessed motor time series. (b) unprocessed sensory time series. (c) processed sensory time series. (d) unprocessed motor and processed sensory time series.

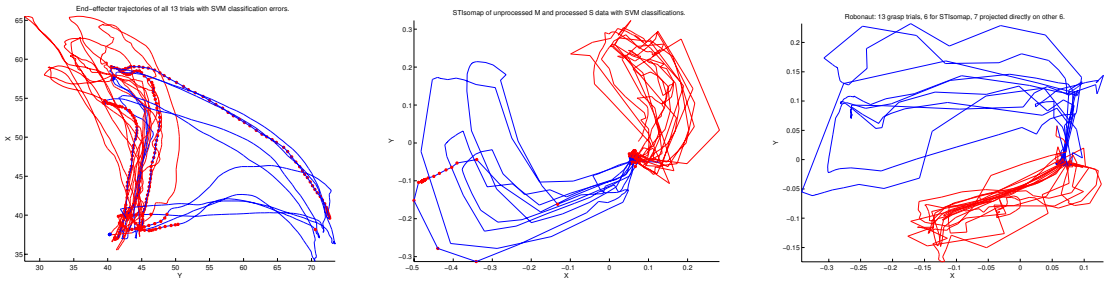

Fig. 6. In (a)-(b) a red * is the location of a point on a successful trajectory that was misclassified by the SVM and blue star is an incorrectly classified point on an unsuccessful trajectory. (b)-(c) were generated from the same training and test set of vectors. (a) vectors misclassified by SVM plotted on the end-effecter (real-world) trajectory. (b) Vectors misclassified by SVM plotted on STI Trajectory (Unprocessed motor, processed sensor). (c) Projection of 3 successful and 4 unsuccessful trajectories (thick lines) onto the STI embedding of 2 successful and 4 unsuccessful trajectories (thin lines).

[15] O. C. Jenkins, "Data-driven derivation of skills for autonomous humanoid agents," Ph.D. dissertation, University of Southern California, Robotics Research Laboratory, Center for Robotics and Embedded Systems, Computer Science Department, University of Southern California, 941 W. 37th Place, Los Angeles, CA 90089 USA, 2003.
[16] J. B. Tenenbaum, V. de Silva, and J. C. Langford, "A global geometric framework for nonlinear dimensionality reduction," *Science*, vol. 290, pp. 2319–2323, 22 December 2000.
[17] R. O. Duda, P. E. Hart, and D. G. Stork, *Pattern Classification (2nd Edition)*. Wiley-Interscience, 2000.
[18] T. Cox and M. Cox, *Multidimensional Scaling*. London: Chapman and Hall, 1994.
[19] S. Roweis and L. Saul, "Nonlinear dimensionality reduction by locally linear embedding," *Science*, vol. 290, no. 5500, pp. 2323–2326, Dec. 2000.
[20] M. Asada, M. Ogino, S. Matsuyama, and J. Ooga, "Imitation learning based on visuo-somatic mapping," in *Proceedings of 9th International Symposium on Experimental Robotics*, vol. CD-ROM. Singapore: Springer-Verlag, June 2004.
[21] K. F. MacDorman, R. Chalodhorn, and M. Asada, "Periodic nonlinear principal component neural networks for humanoid motion segmentation, generalization, and generation," in *Proceedings of the Seventeenth International Conference on Pattern Recognition*. Cambridge, UK: International Association for Pattern Recognition, Aug. 2004, pp. 537–540.
[22] N. Cristianini and J. Shawe-Taylor, *An Introduction to Support Vector Machines and other kernel-base learning methods*. Cambridge University Press, 2000.
[23] R. Pelossof, A. Miller, P. Allen, and T. Jebara, "An svm learning approach to robotic grasping," in *Proceedings of the 2004 IEEE International Conference on Robotics and Automation (ICRA 2004)*, Apr. 2004, pp. 3212–3218.
[24] R. O. Ambrose, H. Aldridge, R. S. Askew, R. R. Burridge, W. Bluethmann, M. Diftler, C. Lovchik, D. Magruder, and F. Rehnmark, "Robonaut: Nasa's space humanoid," *IEEE Intelligent Systems*, vol. 15, no. 4, pp. 57–63, July 2000.
[25] Robonaut Development Team, "Robonaut avionics," NASA Johnson Space Center, http://robonaut.jsc.nasa.gov/Avionics.htm, Tech. Rep., July 2004.
[26] V. N. Vapnik, *Statistical Learning Theory*. New York: Wiley, 1998.
[27] O. C. Jenkins and M. J. Matarić, "A spatio-temporal extension to isomap nonlinear dimension reduction," in *The International Conference on Machine Learning (ICML 2004)*, Banff, Alberta, Canada, July 2004, pp. 441–448. [Online]. Available: http://www.cs.brown.edu/~cjenkins/papers/cjenkins_stisomap.pdf
[28] C. R. Giardina and E. R. Dougherty, *Morphological Methods in Image and Signal Processing*. Englewood Cliffs: Prentice-Hall, 1988.
[29] C.-W. Hsu, C.-C. Chang, and C.-J. Lin, "A practical guide to support vector classification," Department of Computer Science, National Taiwan University, Tech. Rep., 2003. [Online]. Available: http://www.csie.ntu.edu.tw/~cjlin/papers/guide/guide.pdf